

Electric Tuning of Magnetic Anisotropy and Exchange Bias of $\text{La}_{0.8}\text{Sr}_{0.2}\text{CoO}_3/\text{La}_{0.67}\text{Sr}_{0.33}\text{MnO}_3$ Bilayer Films

Jinghua Song,^{1,2} Yuansha Chen,^{1,3,*} Xiaobing Chen^{1D},^{1,2} Tahira Khan,^{1,2} Furong Han,^{1,2} Jine Zhang,^{1,2} Hailin Huang,^{1,2} Hui Zhang,^{1,2} Wenxiao Shi,^{1,2} Shaojin Qi,^{1,2} Fengxia Hu,¹ Baogen Shen,¹ and Jirong Sun^{1D}^{1,2,4,5,†}

¹ Beijing National Laboratory for Condensed Matter Physics and Institute of Physics, Chinese Academy of Sciences, Beijing 100190, China

² School of Physical Sciences, University of Chinese Academy of Sciences, Beijing 100049, China

³ Fujian Innovation Academy, Chinese Academy of Sciences, Fuzhou, Fujian 350108, China

⁴ Songshan Lake Materials Laboratory, Dongguan, Guangdong 523808, People's Republic of China

⁵ Spintronics Institute, University of Jinan, Jinan, Shandong, 250022, People's Republic of China



(Received 24 March 2020; revised 25 May 2020; accepted 27 July 2020; published 21 August 2020)

Heterostructures composed of dissimilar perovskite oxides with different properties provide an opportunity to observe emergent phenomena, and have promising applications. A key feature of oxide heterostructures is interfacial electronic and orbital reconstruction. In this paper, we demonstrate a dramatic variation in magnetic anisotropy caused by electric tuning of the charge-transfer process in a $\text{La}_{0.8}\text{Sr}_{0.2}\text{CoO}_3/\text{La}_{0.67}\text{Sr}_{0.33}\text{MnO}_3$ bilayer structure. By repeatedly changing the valence state of Co ions in the $\text{La}_{0.8}\text{Sr}_{0.2}\text{CoO}_3$ top layer using ionic-liquid gating, reversible switching of the magnetic easy axis of the bottom $\text{La}_{0.67}\text{Sr}_{0.33}\text{MnO}_3$ layer between the out-of-plane and the in-plane direction is achieved, accompanying a modulation of the interfacial exchange coupling. Mn-to-Co charge transfer and its effect on the interfacial orbital occupancy are further confirmed by x-ray absorption spectroscopy and x-ray-linear-dichroism analysis. The considerable interfacial charge transfer causes an overlap of the Mn and Co $3d$ orbitals, resulting in orbital reconstruction in the $\text{La}_{0.67}\text{Sr}_{0.33}\text{MnO}_3$ layer and thus magnetic anisotropy. This work demonstrates a promising method for tuning the orbital occupancy and related properties of perovskite heterostructures.

DOI: 10.1103/PhysRevApplied.14.024062

I. INTRODUCTION

As typical systems with strong electron correlations, transition-metal oxides (TMOs) with the perovskite structure exhibit abundant interesting phenomena, such as the colossal magnetoresistance effect, high- T_c superconductivity, a high degree of spin polarization, and effects associated with charge and orbital ordering [1–4]. The combination of two or more different perovskite oxides in artificial heterostructures has demonstrated fascinating electronic and magnetic properties different from those of their bulk counterparts. Furthermore, diverse functionalities have been displayed when such heterostructures are subjected to external stimuli, and these functionalities show great potential in application areas such as spintronics, sensors, and high-density data storage [5–7]. In previous work, numerous investigations have focused on the exotic physics of the interlayer coupling, such as

exchange bias, charge transfer, magnetoelectric coupling, and strain-induced orbital reconstruction [8–11]. However, efficient tuning of the interfacial coupling by external stimuli and the resulting effects have been less investigated. More importantly, some of these effects are of great significance. For example, the reversible electric tuning of the magnetic properties of oxide heterostructures is a primary prerequisite for designing low-power-consumption magnetoelectric devices [12].

$\text{La}_{0.67}\text{Sr}_{0.33}\text{MnO}_3$ (LSMO) is an ideal TMO for building artificial heterostructures due to its high Curie temperature ($T_c \sim 350$ K) and half-metallicity [13]. As is well documented, the electron occupancy of the Mn $3d$ orbitals has a strong effect on the transport and magnetic properties of LSMO [14]. The Jahn-Teller distortion of the MnO_6 octahedra in bulk LSMO lifts the degeneracy of the $d_{x^2-y^2}$ and $d_{3z^2-r^2}$ orbitals, leading to a magnetocrystalline anisotropy of approximately 1.8×10^4 erg/cm³ [15]. For LSMO epitaxial films, the substrate-induced strain also dramatically influences the distortion of the MnO_6 octahedra and thus the electron population in the e_g orbitals,

*yschen@aphy.iphy.ac.cn

†jrsun@iphy.ac.cn

resulting in a relatively large magnetic anisotropy (MA) of $5\text{--}10 \times 10^4$ erg/cm³ [16,17]. In general, an in-plane (IP) tensile strain in a (001)-oriented LSMO film favors a $d_{x^2-y^2}$ occupancy, supporting an IP MA. In contrast, a compressive strain favors a $d_{3z^2-r^2}$ occupancy, leading to a perpendicular magnetic anisotropy (PMA) [18]. The latter case is of special importance in applications to data storage and in magnetic tunnel junctions [19] and the magnetic proximity effect [20]. As a result, electric tuning of this effect has been keenly pursued in recent years [21]. Much effort has been devoted to electrical control of the MA, such as by piezoelectrically distorting ferromagnetic-piezoelectric hybrids, electrically altering the MA via magnetoelectric coupling in multiferroics, modulating the carrier density to cause an electronic phase transition, and so on [22–24].

Recently, we explored an unexpected PMA in superlattices and trilayer films based on a LSMO/LaCoO_x (LCO) heterostructure that occurs even though the heterostructure is in an IP tensile state [25]. Indeed, we confirmed that the LSMO/LCO interlayer coupling would cause a unique orbital reconstruction at the interface, and thus a PMA. It is worth noting that, by doping with Sr, the cobaltates $\text{La}_{1-x}\text{Sr}_x\text{CoO}_x$ (LSCO) are obtained, which exhibit a distinct magnetoelectronic phase separation as well as excellent ionic conductivity and catalytic activity [26–28]. Thus, the oxygen composition of LSCO can be easily tuned compared with LCO, through the usual treatments such as thermal annealing under different conditions, irradiating with an electron or ion beam, or electrochemical reactions [29–31]. These treatments result in different valence states and spin states of the Co ions in the LSCO. Moreover, this influences the interfacial states in related heterostructures and, further, modulates emergent phenomena associated with the heterointerfaces. Unlike high-temperature annealing and irradiation treatments, which cause coordinated variations in adjacent layers, the ionic-liquid (IL) gating method, applied under ambient temperature and pressure, provides an alternative approach to feasibly controlling the interfacial coupling in oxide heterostructures [32,33].

In this paper, we demonstrate that a bilayer structure with a single LSCO/LSMO interface is sufficient to cause a strong PMA. More importantly, owing to the simple structure, reversible electric tuning of the PMA and exchange bias in LSCO/LSMO bilayer films is realized by repeatedly gating the valence states of the Co ions in the LSCO cap layer using an IL. Positive IL gating rotates the magnetic easy axis of the bilayer films from the out-of-plane (OP) direction to the IP direction, simultaneously reducing and even reversing the exchange bias. In contrast, subsequent negative gating causes the reverse variations. The results of x-ray absorption spectroscopy and x-ray-linear-dichroism analysis indicate that a tunable Mn-to-Co charge transfer, and thus an orbital reconstruction, is responsible for the variation of the magnetic properties of the bilayer films.

This paper reveals a promising method for electric-field modulation of the orbital occupancy and related properties of manganites.

II. EXPERIMENT

A. Sample preparation and characterization

High-quality La_{0.8}Sr_{0.2}CoO₃/La_{0.67}Sr_{0.33}MnO₃ bilayer films are epitaxially grown on (001)-oriented (LaAlO₃)_{0.3}(SrAl_{0.5}Ta_{0.5}O₃)_{0.7} (LSAT) substrates by the technique of pulsed laser deposition (KrF, $\lambda = 248$ nm). LSMO and LSCO bare films are also prepared for comparison. In the deposition process, the substrate is kept at 700 °C, and the oxygen pressure is set to 30 Pa. The fluence of the laser pulse is 1.6 J/cm², and the repetition rate is 2 Hz. A LSMO layer is first deposited on the substrate, and then a LSCO layer is grown on the LSMO. After deposition, the sample is cooled to room temperature naturally in the furnace without changing the oxygen pressure. The film thickness is determined by the deposition time. The deposition rate is 1.4 nm/min for the LSMO layer and 1 nm/min for the LSCO layer, which is calibrated by the technique of small-angle x-ray reflectivity (XRR) (see Fig. S1 in the Supplemental Material [34]). Following this procedure, a superlattice (SL) sample with a structure [LSCO(4 u.c.)/LSMO(4 u.c.)]₁₀ (where “u.c.” denotes “unit cell”) is also prepared for measurements by x-ray absorption spectroscopy (XAS) and x-ray linear dichroism (XLD).

The surface morphology of the bilayer film is measured with an atomic force microscope (AFM) (SPI 3800N, Seiko). The crystal structure is determined with a high-resolution x-ray diffractometer (D8 Discover, Bruker) with Cu $K\alpha$ radiation. The magnetic properties are measured with a Quantum Designed vibrating sample magnetometer (VSM-SQUID) in a temperature range of 5–380 K. A magnetic field is applied along the IP or the OP direction of the (001) film. For the IL-gating experiments, a Pt/Ti/SiO₂/Si plate and the LSMO layer are used as top and bottom electrodes, respectively [Fig. 2(a)]. The commercial ionic liquid *N,N*-diethyl-*N*-(2-methoxyethyl)-*N*-methylammonium bis (trifluoromethylsulfonyl) imide is used in all IL-gating experiments. The sample is first electrically gated at room temperature for a few minutes, and then put into the VSM-SQUID chamber and cooled in a given magnetic field to a preset temperature for the measurement of magnetic loops. A thermomagnetic curve is collected during the cooling process.

The XAS measurements are performed at the BL08U1A beamline at the Shanghai Synchrotron Radiation Facility at room temperature in a total-electron-yield mode. As shown in the inset of Fig. 5, XLD spectra are measured for two polarization directions of linearly polarized x-rays, which are varied by rotating the x-ray incidence angle, with values of 90° and 30° corresponding to the IP direction ($\mathbf{E} \parallel a$ or b , I_{ab}) and the OP direction ($\mathbf{E} \parallel c$, I_c), respectively,

where \mathbf{E} is the electric field of the x-rays, a , b , and c are the axes of the sample, and I_{ab} and I_c are the absorption intensities along the corresponding directions. The spectra are normalized by dividing the experimental data by a factor that makes the L_3 preedge and L_2 postedge have identical intensities for the two polarizations. After that, the preedge spectrum region is set to zero, and the peak at the L_3 edge is set to unity. The XLD is the difference between the two measurements ($I_{ab} - I_c$), and probes the occupation of the e_g orbital of the Mn (or Co) ions in the LSMO (or LSCO) sublayer. The measurement temperature is 300 K.

III. RESULTS AND DISCUSSION

Figure 1(a) shows the surface morphology of an as-grown LSCO(4.5 nm)/LSMO(4.5 nm) bilayer film

grown on a (001)-oriented LSAT substrate. The root-mean-square (rms) surface roughness is approximately 0.4 nm over an area of $5 \mu\text{m} \times 5 \mu\text{m}$, showing the excellent smoothness and uniformity of the film. Figure 1(b) shows x-ray diffraction (XRD) spectra of a LSMO(6 nm) single film, a LSCO(6 nm) single film, and a LSCO(6 nm)/LSMO(6 nm) bilayer film. The clear thickness fringes around the (002) peak demonstrate the good layer-by-layer epitaxial growth of the film. According to a previous report, the lattice parameter of bulk LSMO is 3.876 Å, which is slightly larger than that of the LSAT substrate ($a = 3.868 \text{ \AA}$) [35]. Thus, a LSMO film is subjected to a weak compressive stress when deposited on (001) LSAT. Differently, the LSCO layer, with a bulk lattice constant of 3.82 Å, is subjected to a tensile stress [36]. These features agree with the θ - 2θ XRD patterns

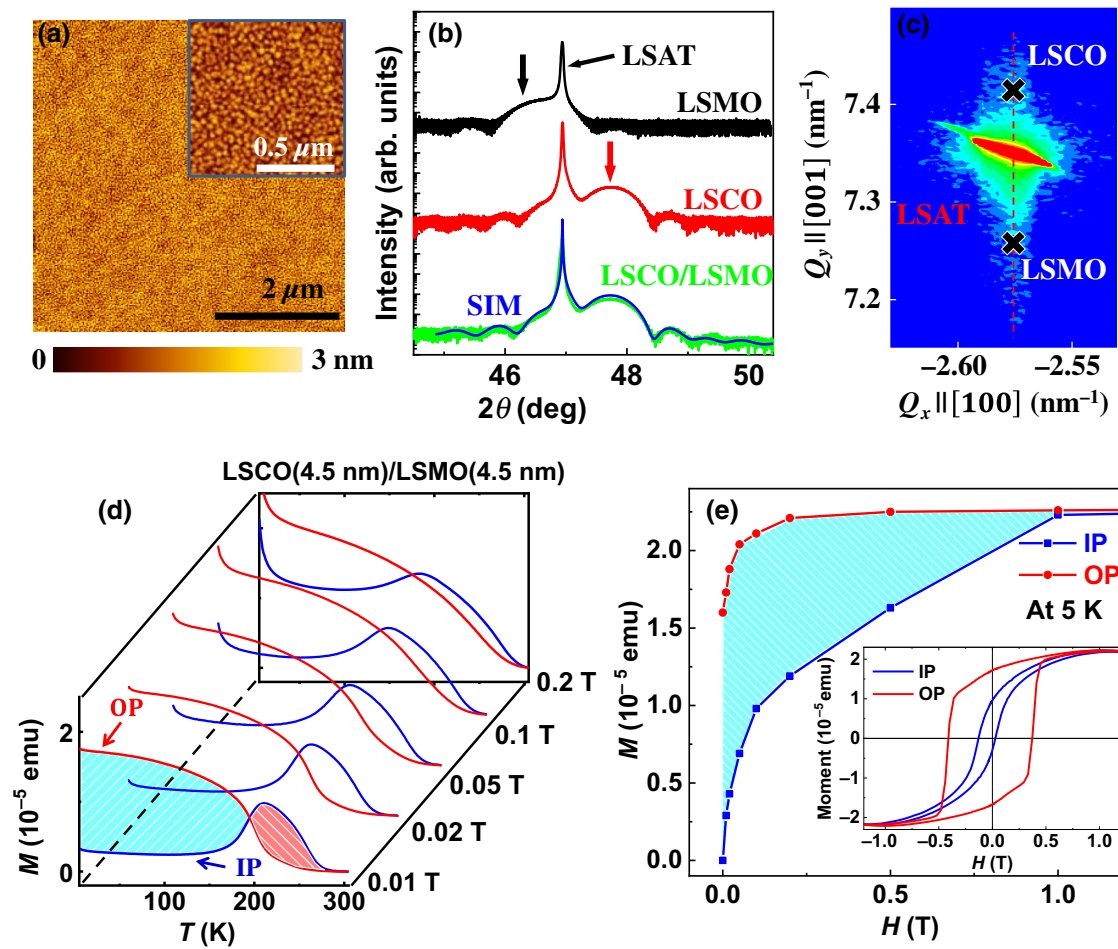


FIG. 1. (a) AFM image ($5 \mu\text{m} \times 5 \mu\text{m}$) of the as-prepared LSCO (4.5 nm)/LSMO(4.5 nm) bilayer film. The inset shows an enlarged image over an area of $1 \mu\text{m} \times 1 \mu\text{m}$. The rms roughness is approximately 0.4 nm. (b) OP θ - 2θ patterns of a LSMO(6 nm) single film, a LSCO(6 nm) single film, and a LSCO(6 nm)/LSMO(6 nm) bilayer film grown on (001)-oriented LSAT substrates. The good agreement between the simulation curve (SIM, blue) and the experimental data (green) indicates the good periodic layered structure of the bilayer film. (c) RSM of the (103) reflection for the bilayer film. (d) Temperature-dependent magnetization (M - T) curves of a LSCO (4.5 nm)/LSMO (4.5 nm) bilayer film measured under different magnetic fields (0.01–0.2 T). (e) Magnetic moment as a function of magnetic field extracted from the M - T curves in (d) at $T = 5 \text{ K}$. The blue-shaded area in (e) corresponds to a PMA energy that is consistent with the direct measurements of the magnetic loops shown in the inset.

in Fig. 1(b). To determine the IP strain state further, reciprocal-space mapping (RSM) of the (103) reflection of the LSCO(6 nm)/LSMO(6 nm) bilayer film is done, and the result is shown in Fig. 1(c). The diffraction peak of the LSMO (or LSCO) sublayer (marked by black crosses) is located just below (or above) that of the LSAT, aligning vertically with that of the substrate. Such a result indicates that the bilayer film is fully strained by the substrate, i.e., either the LSMO or the LSCO sublayer has exactly the same IP lattice constant as the substrate, like the corresponding bare films.

In order to investigate the magnetic properties, temperature-dependent magnetization (M - T) curves of the as-grown films are measured under a magnetic field applied along either the IP or the OP direction. Typical M - T curves of the LSCO (4.5 nm)/LSMO(4.5 nm) bilayer are presented in Fig. 1(d). The MA of the bilayer film is complicated, especially in low magnetic fields. As shown, when the applied field is low (0.01 T), the IP magnetic moment shows a rapid increase when the sample is cooled from 280 to 210 K, whereas the OP moment does not. This means an IP MA in the high-temperature region. However, further cooling leads to a turning point from an increase to a decrease in the IP M - T curve. Correspondingly, the OP component first grows rapidly immediately after the turning point and then gradually approaches a saturation state. At 5 K, the OP magnetic moment is nearly 7 times as large as the IP moment, suggesting a strong PMA at low temperatures (less than 210 K). Obviously, a spin reorientation occurs below 210 K, resulting in a rotation of the easy axis from the IP to the OP direction. For comparison, the magnetic properties of a bare LSCO film (10 nm thick) are measured, giving no magnetic signal [see Fig. S2(a) in the Supplemental Material [34]], although the bulk counterpart shows ferromagnetic (FM) behavior below 160 K [37]. This is consistent with previous results that tensile strain suppresses the FM ordering of LSCO thin films, resulting in a spin-glass state with small FM clusters [38]. Therefore, the PMA of the LSCO/LSMO bilayer sample stems totally from the LSMO sublayer. Notably, spin reorientation is not observed in a bare LSMO film with the same thickness as the LSMO layer in the bilayer sample [see Fig. S2(b) in the Supplemental Material [34]]. According to Fig. 1(c), the LSMO sublayer in the bilayer sample is strained to the same degree as the LSMO single film. The sharp contrast in the MA between the bare LSMO layer and the LSCO/LSMO bilayer sample implies the occurrence of an interfacial effect. That is, the interlayer coupling plays an important role in determining the PMA in the LSCO/LSMO bilayer system. It is worth noting that with increasing thickness of the LSMO, the critical temperature for spin reorientation decreases gradually in LSCO/LSMO bilayers (see Fig. S3 in the Supplemental Material [34]). Meanwhile, the difference between the magnetic moments along the OP and the IP directions is reduced, meaning

that the PMA decreases as the thickness of the LSMO layer grows. This is a typical feature of an interfacial effect.

The PMA energy of the LSCO (4.5 nm)/LSMO (4.5 nm) film is calculated in Fig. 1(e). Figure 1(e) is composed of curves of the magnetization characteristics (M - H curves) at 5 K, extracted from M - T curves measured with different magnetic fields \mathbf{H} . The magnetization \mathbf{M} in the OP direction quickly reaches its saturation value at 0.2 T, whereas it grows much more slowly in the IP direction. The blue-shaded area enclosed by these two M - H curves is used to quantitatively describe the MA energy of the bilayer system. A large anisotropy constant $K_{\text{eff}} = 9.8 \times 10^5 \text{ emu/cm}^3$ is obtained for the LSCO (4.5 nm)/LSMO (4.5 nm) film, where a positive sign implies that the easy axis is along the OP direction. The anisotropy constant can also be estimated from the direct measurements of the magnetic loops, as shown in the inset of Fig. 1(e), and this gives essentially the same result ($9.8 \times 10^5 \text{ emu/cm}^3$). Such a value far exceeds the conventional anisotropy energy caused by the magnetoelastic coupling ($8.4 \times 10^4 \text{ erg/cm}^3$) or the magnetocrystalline anisotropy ($1.8 \times 10^4 \text{ erg/cm}^3$) of the LSMO single film, as mentioned above. A similar unexpected PMA is also identified in superlattices and trilayer films based on a LCO/LSMO heterostructure [24]. Although the anisotropy constant for a single LSCO/LSMO interface is smaller than that of a LCO/LSMO trilayer sample with two interfaces (approximately $5.6 \times 10^6 \text{ erg/cm}^3$), we clearly demonstrate that one single LSCO/LSMO interface in a bilayer structure is sufficient to cause a strong PMA. Compared with LCO, the LSCO sublayer shows nearly no magnetic signal [39] and has a higher oxygen ionic conductivity [26,27]. Thus, it is more convenient to tune the interfacial coupling and, further, the MA of the system through manipulating the oxygen stoichiometry of the LSCO sublayer.

Next, we turn our attention to the electric tuning of the LSCO/LSMO bilayer system. A typical LSCO (4.5 nm)/LSMO (4.5 nm) sample is selected for IL gating. The experimental setup is shown in Fig. 2(a). The IL is dropped onto the upper surface of the LSCO layer, and an electric field is applied between the top Pt layer and the bottom LSMO sublayer. As is well documented, besides electrostatic gating of the film by double-layer capacitors, IL gating also causes an oxidation-reduction reaction in thin-film samples [31]. Based on the fact that LSCO has an oxygen diffusion constant several orders of magnitude higher than that of LSMO [40], with careful management of the bias voltage and gating time, it is possible to control the oxygen stoichiometry and the Co-ion valence or spin state of the LSCO cap layer while keeping the bottom LSMO layer basically unaffected. Figure 2(b) shows XRD spectra of a LSCO/LSMO bilayer film taken in different intermediate states during a complete electric cycle. According to Fig. 1(b), the film peak on the right side

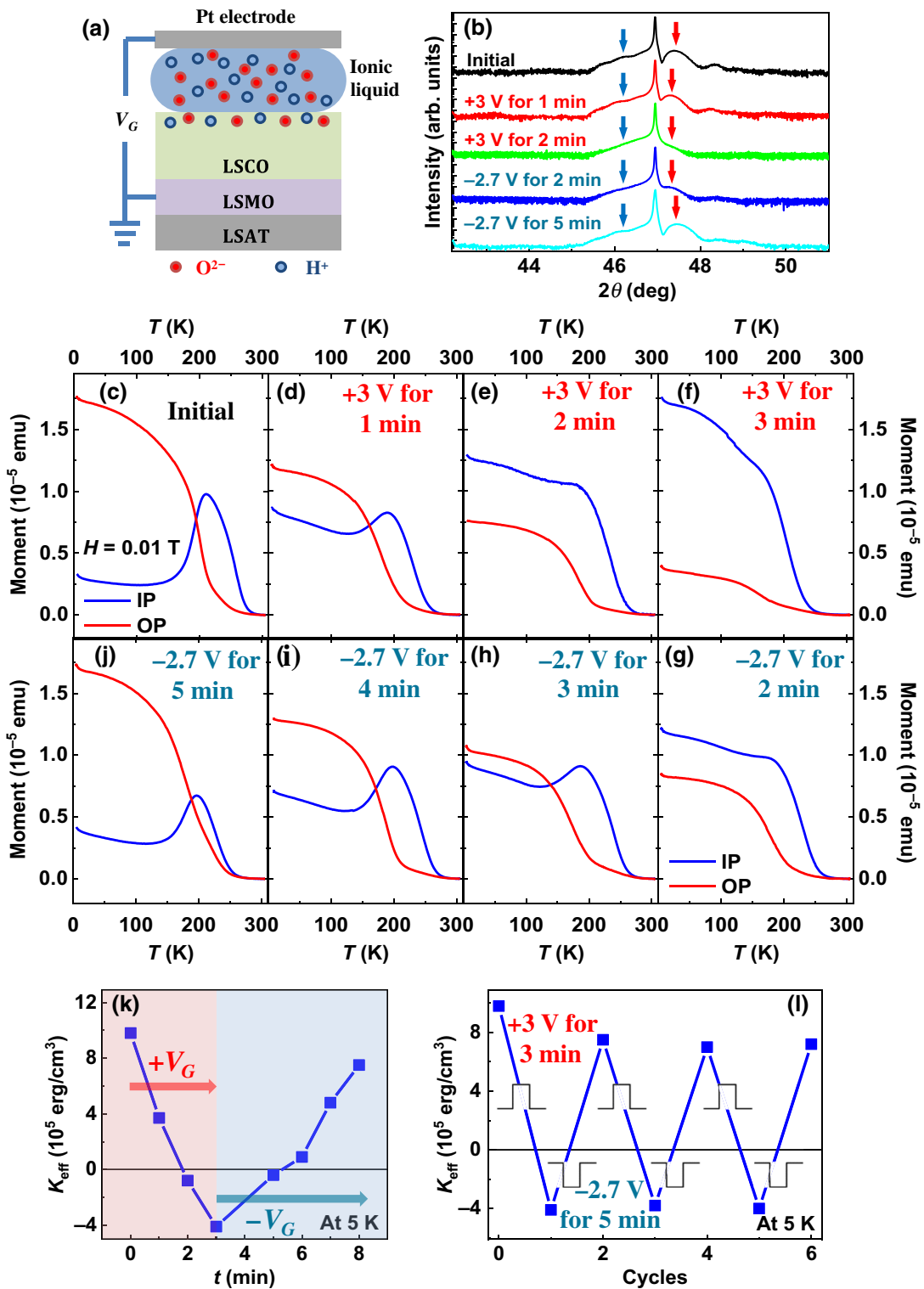


FIG. 2. (a) Experimental setup for the IL gating performed on the LSCO/LSMO bilayer. (b) XRD spectra of the LSCO/LSMO bilayer film measured in the initial state and different intermediate states during one tuning cycle. (c) $M-T$ curves of a LSCO(4.5 nm)/LSMO(4.5 nm) bilayer film measured in the initial state and (d)–(f) different positively gated states: +3 V biasing for 1, 2, and 3 min, respectively. (g)–(j) $M-T$ curves of the same LSCO/LSMO bilayer film measured in the following negative gating process: -2.7 V biasing for 2, 3, 4, and 5 min, respectively. A magnetic field of 0.01 T is applied along the IP direction (blue lines) or the OP direction (red lines). (k) Calculated K_{eff} of the same sample as a function of the tuning time t . (l) Variation of K_{eff} during three repeated electric tuning cycles. The rectangular waves indicate the gating bias for each gating procedure: a positive gating of +3 V for 3 min and a negative gating of -2.7 V for 5 min. The anisotropy constants are estimated at 5 K.

of the substrate peak, marked by red arrows, is largely determined by the LSCO layer. When a positive bias is applied to the bilayer film, the intensity of the right peak decreases quickly with biasing time, and the peak position also moves slightly to lower angles. However, when the polarity of the gating voltage is reversed, the intensity gradually rises and finally recovers to the initial state after enough biasing time. Notably, the LSMO peak, represented by the peak to the left of the substrate peak (marked by blue arrows), is almost unchanged during the electric cycling, which means that the bottom LSMO layer is basically not affected by the IL gating. According to the experimental results, a bias sequence consisting of a positive voltage of +3 V for 3 min and a negative voltage of -2.7 V for 5 min is appropriate for the present sample, yielding well-repeated structural cycles for the LSCO layer without affecting the LSMO.

Accompanying the structural variations, the magnetic properties of the LSCO/LSMO bilayer film are tuned at the same time. Figures 2(c)–2(j) show a series of M - T curves measured at different gating times during one complete tuning cycle. Under a positive electric bias of +3 V, the low-temperature part of the IP M - T curve (less than 210 K) shifts upwards with the gating time, whereas the OP M - T curve moves down [Figs. 2(c)–2(f)]. The magnetic moment in the IP direction exceeds that in the OP direction when the gating time exceeds 2 min, indicating a transition of the easy axis from the OP direction to the IP direction. More importantly, such electric tuning of the MA is fully reversible. Under a negative bias of -2.7 V, the M - T curves measured in the two directions gradually return to their initial shapes [Figs. 2(g)–2(j)], and, accordingly, the PMA is recovered. In Fig. 2(k), we show K_{eff} as a function of the gating time t . K_{eff} decreases from 9.8×10^5 erg/cm 3 to -4.1×10^5 erg/cm 3 after a 3 min positive gating and then returns to 7.5×10^5 erg/cm 3 after a subsequent 5 min negative gating. That is to say, IL gating causes a variation in the anisotropy energy as large as approximately 1.4×10^6 erg/cm 3 . It is of great importance that such electric tuning of the MA is repeatable. Figure 2(l) gives the calculated K_{eff} for three switching cycles. The corresponding M - T curves are given in Fig. S4 in the Supplemental Material [34]. Although the anisotropy energy displays a slight degeneration after the first cycle, it tends to a stable value in subsequent cycles.

The above experiments demonstrate the important role of interfacial coupling in modifying the PMA of the bilayer sample. In addition to the PMA, we observe an exchange bias in the bilayer sample and its variation under IL gating. Figures 3(a)–3(c) show M - H curves of the LSCO(4.5 nm)/LSMO(4.5 nm) bilayer film in three typical states: the initial state, a positively tuned (+3 V for 3 min) state, and the fully restored state. The film is first cooled from 330 to 5 K in the presence of a magnetic field of +3 T and then measured at 5 K by cycling the magnetic

field between +1.2 and -1.2 T. Notable changes in the IP and OP hysteretic loops take place during the electric tuning, mainly in the squareness and the coercivity. As shown in Fig. 3(a) for the initial state, the OP M - H curve shows much better squareness than that for the IP direction, tallying with the fact that easy axis lies in the OP direction, which is confirmed by the M - T curves in Fig. 2(c). Here, the value of the coercivity field H_c is defined by $(H_{c1} + H_{c2})/2$, and the exchange bias H_{EB} is defined by $(-H_{c1} + H_{c2})/2$, where H_{c1} and H_{c2} are the absolute values of the left and right coercive fields, respectively. In the initial state, the coercive field is much larger for the OP magnetic loop than for the IP loop (3900 vs 800 Oe). A careful analysis further indicates that both M - H curves show a shift to the left, implying the presence of exchange bias. A direct calculation gives $H_{\text{EB}} = -180$ Oe for the OP direction and -500 Oe for the IP direction. The negative sign of H_{EB} means that the interfacial coupling between the LSCO and the LSMO sublayer is ferromagnetic. After positive IL gating, the magnetic loops for the IP and OP directions exchange their shapes [Fig. 3(b)]. This is due to the rotation of the easy axis from OP to IP by the IL gating. More interestingly, the negative H_{EB} shifts gradually to zero and even becomes slightly positive (+23 Oe for the OP direction and +55 Oe for the IP direction) after 3 min of positive biasing. Then, the following negative IL gating exerts a reversible effect on the hysteresis loops [Fig. 3(c)]. The two M - H curves are essentially restored to their initial shape, with a negative value of H_{EB} , accompanied by recovery of the PMA. More details of the variation of H_c and H_{EB} in one complete cycle of electric tuning are summarized in Figs. 3(g) and 3(h). The good agreement between the inverted V-shaped H_{EB} and the V-shaped K_{eff} [Fig. 2(k)] reveals the strong relation between the MA and the exchange bias. As is well established, the exchange bias is a direct measurement of the exchange coupling energy at a heterointerface [8]. Thus, the coordinated variations of H_{EB} and K_{eff} imply that the modulation of the interfacial coupling by IL gating is the prime cause of the tuning of the exchange bias as well as of the MA in LSCO/LSMO bilayers.

In order to get further information on the interfacial state, soft XAS and XLD spectra are measured for the Mn and Co L edges. To highlight interfacial effects, a [LSCO(4 u.c.)/LSMO(4 u.c.)] $_{10}$ (SL $_{10}$) superlattice sample is used in the experiment. Figure S5 in the Supplemental Material [34] shows that the SL $_{10}$ sample also has a PMA in the initial state and changes to having an in-plane MA after positive gating. Because of the formation of a dead layer [41], T_c of the SL $_{10}$ sample is significantly lower than that for a single LSMO film with the same thickness as the superlattice. In Fig. 4, we show the XLD spectra of a LSMO single film (a), the initial SL $_{10}$ sample (b), and the positively tuned SL $_{10}$ sample (c). Details of the XLD measurements are given in Sec. II. These data confirm

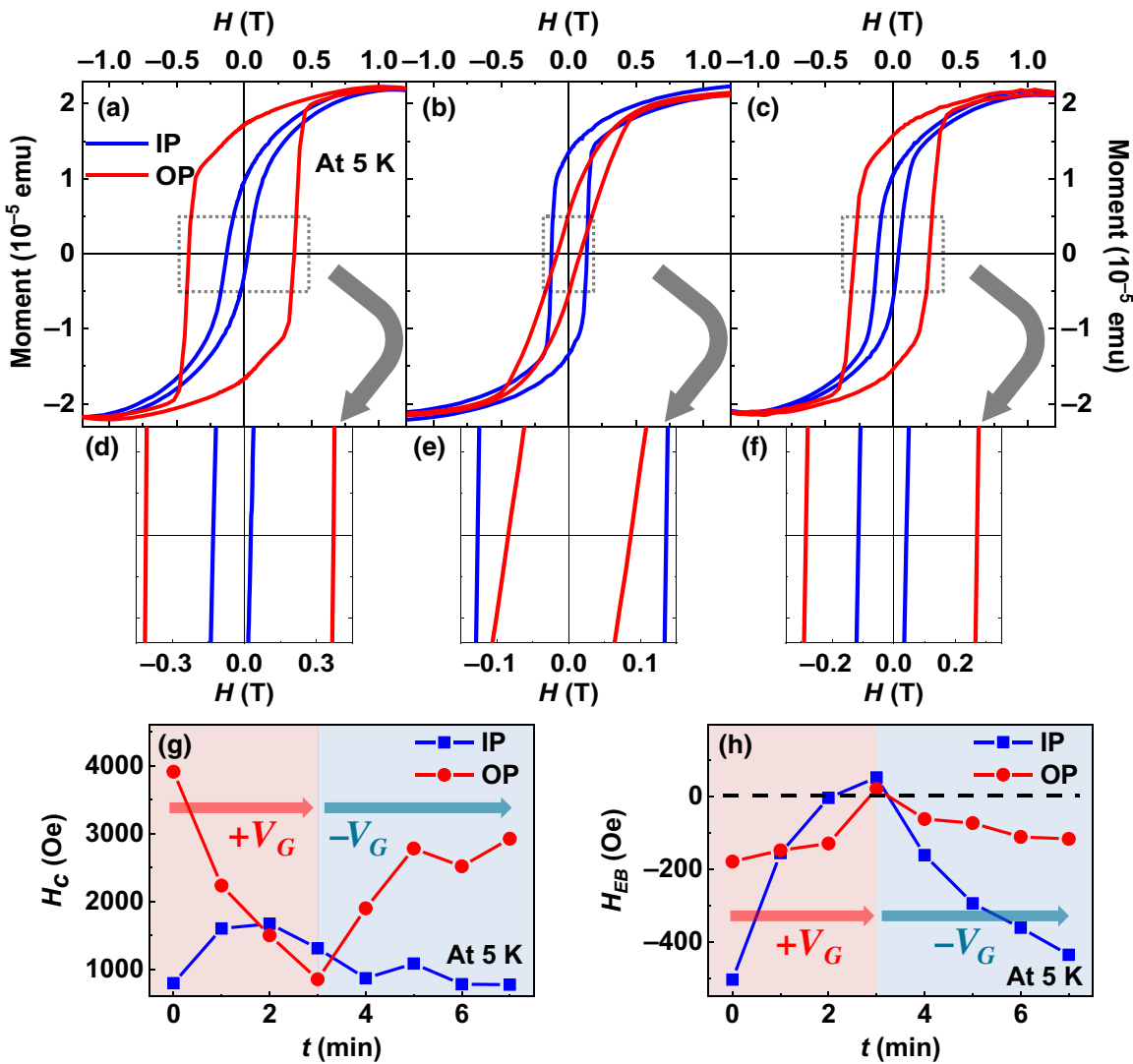


FIG. 3. Hysteresis loops for (a) the initial state, (b) the positively tuned state, and (c) the recovered state of the LSCO(4.5 nm)/LSMO(4.5 nm) bilayer, measured at 5 K with a magnetic field applied along the IP or OP direction after +3 T field-cooling from room temperature. (d)–(f) Corresponding enlarged views of the low-field region. (g),(h) Summary of (g) the coercive field (H_c) and (h) the exchange bias (H_{EB}) of the bilayer film in different tuning states at 5 K.

the existence of orbital reconstruction at the LSCO/LSMO interface. Since the $d_{3z^2-r^2}$ orbital is in the OP direction, while the $d_{x^2-y^2}$ orbital lies in the film plane, the spectral intensities I_c and I_{ab} should be proportional to the hole content in the $d_{3z^2-r^2}$ and $d_{x^2-y^2}$ orbitals, respectively. As reported [18,42,43], the XLD signal around the high-energy L_2 absorption peak (648–660 eV) is very sensitive to the occupancy of the e_g orbitals: larger absorption for one polarization indicates more empty states in the e_g band and thus a lower occupancy. The XLD signals of the Mn spectra shown in Figs. 4(a)–4(c) have an obvious negative peak for the LSMO single film, a positive peak for the initial SL_{10} sample, and a negative peak for the positively biased SL_{10} sample. These experimental results indicate that the preferentially occupied orbitals are $d_{x^2-y^2}$, $d_{3z^2-r^2}$,

and $d_{x^2-y^2}$, respectively, for the three states. According to the Bruno model, the spins of the Mn ions prefer to follow the direction of the orbital momentum [44,45]. That is, the reversible variation of the MA between the OP and IP directions can be ascribed to orbital reconstruction. Similar orbital reconstructions are also observed for Co ions, as shown in Figs. 4(d)–4(e).

To reveal the orbital reconstruction at the LSCO/LSMO interface, Figs. 5(a) and 5(b) compare the XAS spectra of the Mn and Co L edges (both at a 90° incidence angle) measured on the initial SL_{10} sample and the corresponding LSMO or LSCO bare film. As shown, the Mn- L_3 peak displays a shift to the right from the bare LSMO film to the SL_{10} sample (642.4 vs 642.8 eV), while the Co- L_3 peak shifts to a lower binding energy (780.1 vs 779.4 eV). For

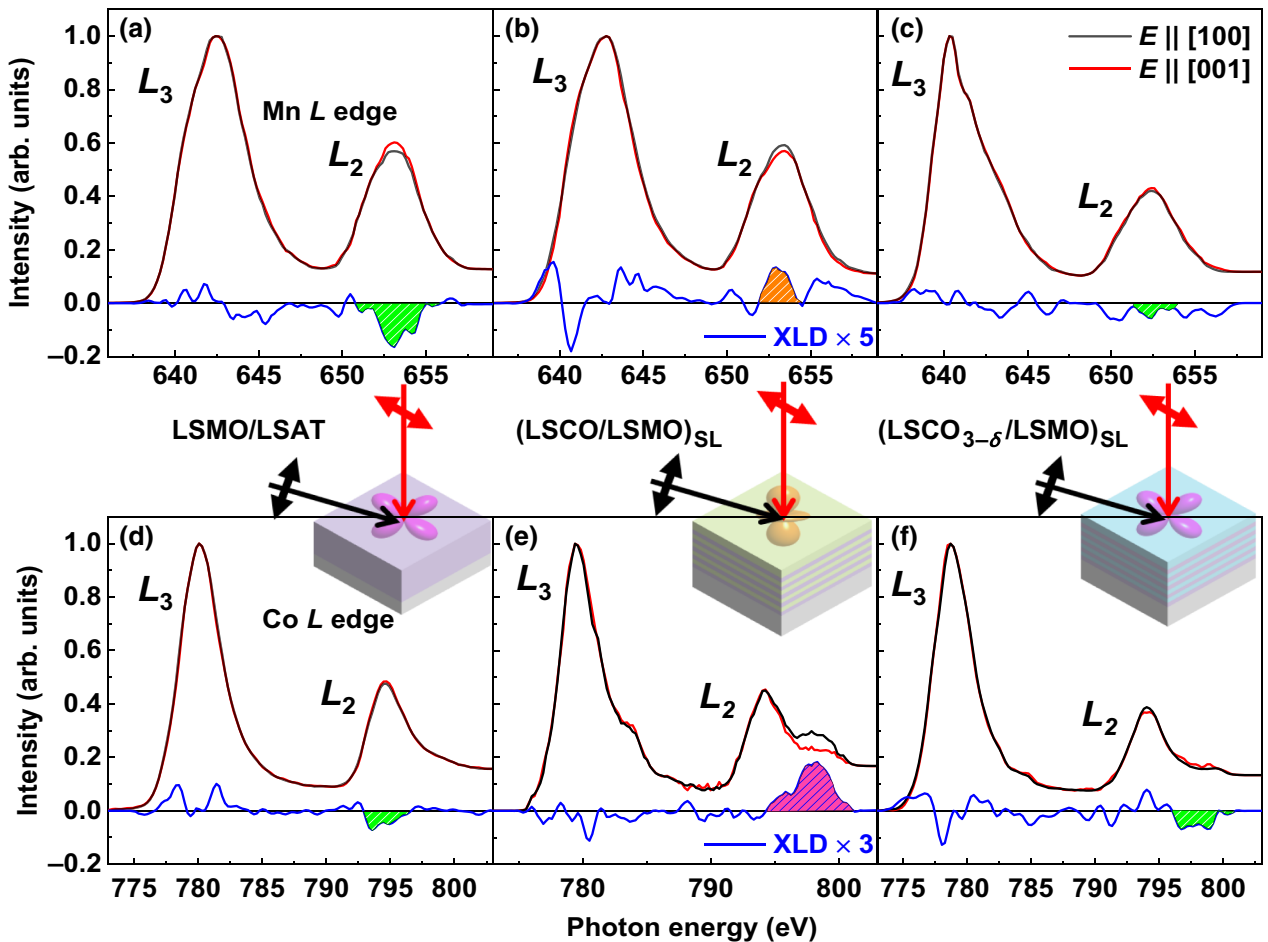


FIG. 4. Normalized XAS spectra of the Mn *L* edge for (a) the LSMO single film, (b) the initial SL₁₀ sample, and (c) the positively tuned SL₁₀ sample, measured with a polarized x-ray beam at different incidence angles (see Sec. II). Each deduced XLD spectrum ($I_{ab} - I_c$) is shown by a blue line. The peak values of the XLD spectra for the LSMO single film, the initial SL₁₀ sample, and the positively tuned SL₁₀ sample are -3.3% , $+2.7\%$, and -1.1% , respectively. The smaller XLD signal for the positively tuned SL₁₀ sample is possibly due to degeneration of the magnetic properties of the LSMO layers caused by the IL gating (see Fig. S5 in the Supplemental Material [34]). (d)–(f) Normalized XAS spectra of the Co *L* edge for a corresponding sample.

the Mn ions, the 0.4-eV peak shift between the SL and the single film is comparable to or greater than that for a LSMO film with a MgO or NdGaO₃ capping layer reported by Valencia *et al.*, which was considered to be an indication of an increase in the Mn⁴⁺ content by about 15%–18% at the interface [46]. For the Co ions, besides the obvious shift towards lower energies opposite to that for the Mn ions, a fingerprint shoulder peak at 775.8 eV occurs in the spectrum of the SL, which is generally due to the appearance of Co²⁺ [47,48]. All these features indicate an increase (decrease) in the valence state of the Mn ions (Co ions) when the LSCO/LSMO interface is formed. Such a variation in valence state implies charge transfer between B-site ions at the interface, which should be electron transfer from Mn³⁺ to Co³⁺ ions here, resulting in Mn⁴⁺-Co²⁺ pairs. As reported, the coupling between the Mn⁴⁺ and Co²⁺ ions is ferromagnetic, based on the superexchange interaction [49]. Thus, the shift of the magnetic loop to the

left for the as-grown heterostructure as shown in Fig. 3(a) is explained by such ferromagnetic coupling. Furthermore, it has been pointed out that the Mn³⁺-to-Co³⁺ charge transfer proceeds via an intermediate O 2p orbital [50]. In our SL sample, orbital overlap should occur between the $d_{3z^2-r^2}$ orbitals of Mn and Co ions via the O 2p_z orbital.

Figure 5(c) is a sketch of the Mn³⁺-to-Co³⁺ charge transfer at the as-grown LSCO/LSMO interface. As shown, the charge transfer causes the formation of Mn-O-Co covalent bonds at the interface, lowering the energy level of $d_{3z^2-r^2}$, leading to more occupation and, in turn, strengthening the interaction. The preferential occupation resulting from the interaction of the $d_{3z^2-r^2}$ orbitals for both the Mn and the Co ions is confirmed by the XAS spectra in Figs. 4(b) and 4(c). According to the Bruno model, this implies a PMA for the as-grown heterostructure, as observed in Fig. 1(d). That is, the PMA and the ferromagnetic exchange bias, which are different aspects

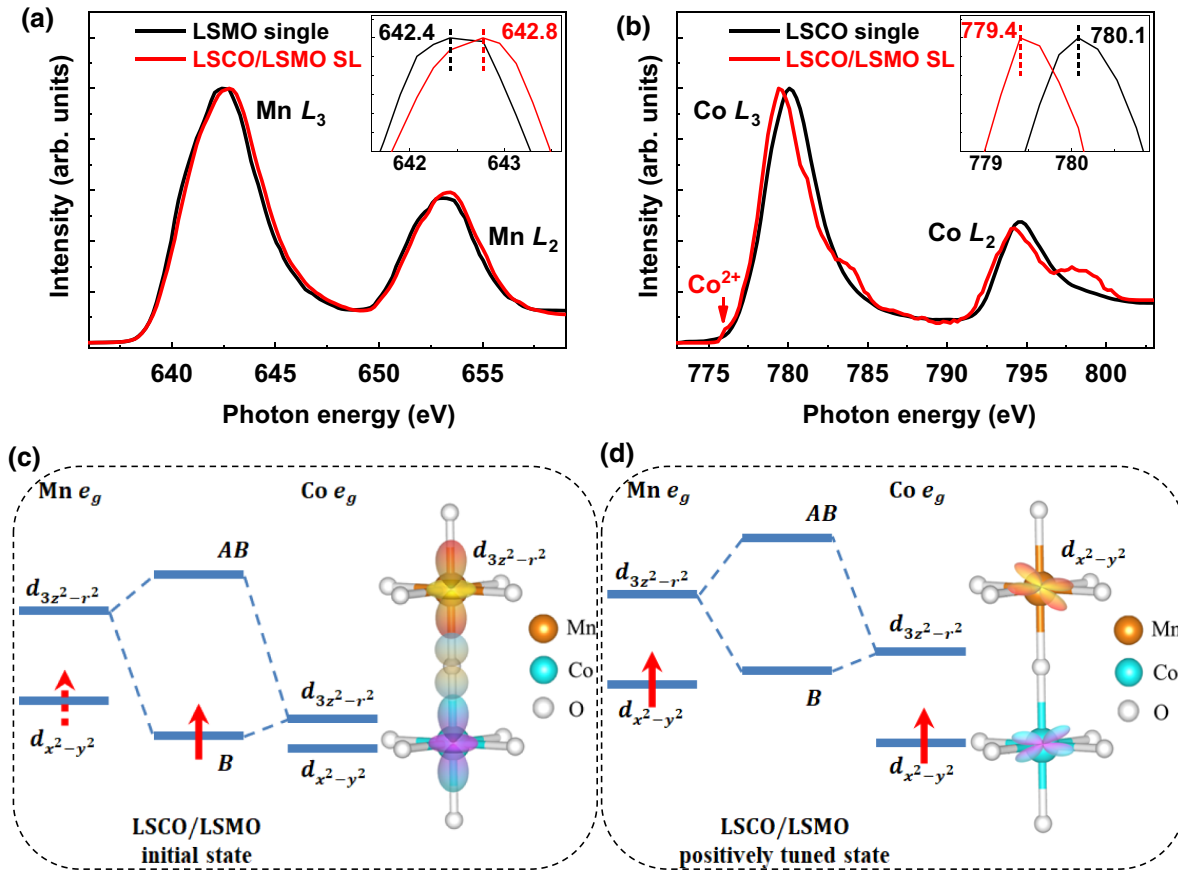


FIG. 5. (a) XAS spectra of the Mn *L* edge for the LSMO single film and the initial SL₁₀ sample. The shift of the Mn-*L*₃ edge to the right is enlarged in the inset. (b) XAS spectra of Co *L* edge for the LSCO single film and the initial SL₁₀ sample. The shift of the Co-*L*₃ edge to the left is enlarged in the inset. (c),(d) Schematic illustration of orbital reconstruction and the formation of molecular orbitals between the interfacial Mn and Co *e_g* orbitals at the interface of a LSCO/LSMO heterostructure in (c) the initial state and (d) the positively tuned state. *AB* and *B* refer to the antibonding and bonding states, respectively, arising from the strong hybridization of the *d*_{3z²-r²} orbitals between the Mn and Co bands.

of the interfacial coupling, can be described in a unified way in the Mn³⁺-to-Co³⁺ charge transfer model. Moreover, the Mn³⁺-to-Co³⁺ model can also explain the effects of IL gating on the bilayer films. Figure S6 in the Supplemental Material [34] shows XAS spectra of the Mn and Co ions in the bilayer film before and after positive gating. The valence state of the Co ions is reduced significantly, which is confirmed by the shift of the Co-*L*₃ peak to the left from 780.0 to 778.7 eV, while the valence state of the Mn ions stays unchanged during the positive gating process. These results coincide with the XRD results in Fig. 2(b). As illustrated in Fig. 5(d), a decreased Co valence state, with a higher Fermi energy, narrows the energy difference between the LSCO and LSMO layers. This restrains the charge-transfer effect accordingly, making the in-plane *d*_{x²-y²} orbitals become the preferred orbitals again, as in the single LSMO film. As shown in Figs. 3(a) and 3(b), the rotation of the easy axis from the OP direction to the IP direction after the positive IL gating is accompanied by a change in the sign of *H*_{EB} from negative to positive.

The positive sign then indicates that antiferromagnetic interactions become slightly dominant after the +3 V gating. During the gating process, mixed valence states Co²⁺, Co³⁺, and Co⁴⁺ for the Co ions and Mn³⁺ and Mn⁴⁺ for the Mn ions are all present at the LSCO/LSMO interface. According to the Goodenough-Kanamori-Anderson rules [50], the Co²⁺-O-Mn⁴⁺ coupling is ferromagnetic, whereas the Co³⁺-O-Mn⁴⁺ and Co²⁺-O-Co³⁺ couplings are antiferromagnetic. Therefore, the competition between these interactions, which varies with the proportions of Co²⁺ and Co³⁺ ions, eventually determines the sign of *H*_{EB} during the IL gating, which turns out to lead to systematic changes in *H*_{EB} during the electric gating shown in Fig. 3(h). Thus, the abnormal PMA and the ferromagnetic exchange bias, as well as the tuning of both of these effects, are united in the Mn³⁺-to-Co³⁺ charge-transfer model. In other words, the interfacial coupling between the Mn and Co ions, i.e., the presence of Mn⁴⁺ and Co²⁺ ions resulting from Mn³⁺-to-Co³⁺ charge transfer at the interface of the LSCO/LSMO heterostructure, is the main origin of

the PMA and the ferromagnetic exchange bias, and of the corresponding electric tuning of these, in the LSCO/LSMO heterostructure system.

IV. CONCLUSION

In summary, a strong PMA is achieved in a simple bilayer structure consisting of a LSCO/LSMO film on a (001) LSAT substrate. Using IL gating, we obtain simultaneous electric tuning of the magnetic anisotropy and exchange bias in such LSCO/LSMO bilayers. The magnetic easy axis is repeatedly switched between the OP and IP directions, and the interfacial exchange coupling displays a corresponding modulation. Furthermore, x-ray absorption spectroscopy and x-ray-linear-dichroism analysis indicate that orbital reconstruction at the LSCO/LSMO interface resulting from Mn-to-Co charge transfer is responsible for the variation of the magnetic properties. Our work demonstrates a possible avenue to achieving control of magnetic states in oxide heterostructures.

ACKNOWLEDGMENTS

This work was supported by National Basic Research of China (Grants No. 2016YFA0300701, No. 2017YFA0206300, and No. 2018YFA0305704), the National Natural Science Foundation of China (Grants No. 11520101002, No. 51972335, No. 1192004, No. 51590880, No. 11934016, and No. 11674378), and the Key Program of the Chinese Academy of Sciences. We also acknowledge Beamline BL08U1A at the Shanghai Synchrotron Radiation Facility (SSRF) for the XAS characterization.

- [1] Y. Tokura and N. Nagaosa, Orbital physics in transition-metal oxides, *Science* **288**, 462 (2000).
- [2] M. Imada, A. Fujimori, and Y. Tokura, Metal-insulator transitions, *Rev. Mod. Phys.* **70**, 1039 (1998).
- [3] J. M. D. Teresa, A. Barthelemy, A. Fert, J. P. Contour, F. Montaigne, and P. Seneor, Role of metal-oxide interface in determining the spin polarization of magnetic tunnel junctions, *Science* **286**, 507 (1999).
- [4] S. Okamoto and A. J. Millis, Electronic reconstruction at an interface between a Mott insulator and a band insulator, *Nature (London)* **428**, 630 (2004).
- [5] E. Dagotto, Complexity in strongly correlated electronic systems, *Science* **309**, 257 (2005).
- [6] H. B. Wu, J. S. Chen, H. H. Hng, and X. W. Lou, Nanosstructured metal oxide-based materials as advanced anodes for lithium-ion batteries, *Nanoscale* **4**, 2526 (2012).
- [7] M. J. Lee, S. I. Kim, C. B. Lee, H. Yin, S. E. Ahn, B. S. Kang, K. H. Kim, J. C. Park, C. J. Kim, I. Song, S. W. Kim, G. Stefanovich, J. H. Lee, S. J. Chung, Y. H. Kim, and Y. Park, Low-temperature-grown transition metal oxide based storage materials and oxide transistors for high-density non-volatile memory, *Adv. Funct. Mater.* **19**, 1587 (2009).
- [8] J. Nogues and I. K. Schuller, Exchange bias, *J. Magn. Magn. Mater.* **192**, 203 (1999).
- [9] V. I. Anisimov, J. Zaanen, and O. K. Andersen, Band theory and Mott insulators: Hubbard U instead of stoner I, *Phys. Rev. B* **44**, 943 (1991).
- [10] C. A. F. Vanz, Electric field control of magnetism in multiferroic heterostructures, *J Phys. Con. Matter.* **24**, 333201 (2012).
- [11] A. Tebano, C. Aruta, S. Sanna, P. G. Medaglia, G. Balestrino, A. A. Sidorenko, R. De Renzi, G. Ghiringhelli, L. Braicovich, V. Bisogni, and N. B. Brookes, Evidence of Orbital Reconstruction at Interfaces in Ultrathin $\text{La}_{0.67}\text{Sr}_{0.33}\text{MnO}_3$ Films, *Phys. Rev. Lett.* **100**, 137401 (2008).
- [12] J. T. Heron, M. Trassin, K. Ashraf, M. Gajek, Q. He, S. Y. Yang, D. E. Nikonorov, Y.-H. Chu, S. Salahuddin, and R. Ramesh, Electric-Field-Induced Magnetization Reversal in a Ferromagnet-Multiferroic Heterostructure, *Phys. Rev. Lett.* **107**, 217202 (2011).
- [13] H. Y. Hwang, S. W. Cheong, N. P. Ong, and B. Batlogg, Spin-Polarized Intergrain Tunneling in $\text{La}_{2/3}\text{Sr}_{1/3}\text{MnO}_3$, *Phys. Rev. Lett.* **77**, 2041 (1996).
- [14] A. M. Haghiri-Gosnet and J. P. Renard, Cmr manganites: Physics, thin films and devices, *J. Phys. D: Appl. Phys.* **36**, R127 (2003).
- [15] Y. Suzuki, H. Y. Hwang, S. W. Cheong, T. Siegrist, R. B. van Dover, A. Asamitsu, and Y. Tokura, Magnetic anisotropy of doped manganite thin films and crystals, *J. Appl. Phys.* **83**, 7064 (1998).
- [16] K. Steenbeck and R. Hiergeist, Magnetic anisotropy of ferromagnetic $\text{La}_{0.7}(\text{Sr}, \text{Ca})_{0.3}\text{MnO}_3$ epitaxial films, *Appl. Phys. Lett.* **75**, 1778 (1999).
- [17] A. Rajapitamahuni, L. Zhang, M A Koten, VR Singh, JD Burton, E Y Tsymbal, JE Shield, and X. Hong, Giant Enhancement of Magnetic Anisotropy in Ultrathin Manganite Films via Nanoscale 1D Periodic Depth Modulation, *Phys. Rev. Lett.* **116**, 187201 (2016).
- [18] D. Pesquera, G. Herranz, A. Barla, E. Pellegrin, F. Bondino, E. Magnano, F. Sanchez, and J. Fontcuberta, Surface symmetry-breaking and strain effects on orbital occupancy in transition metal perovskite epitaxial films, *Nat. Commun.* **3**, 1189 (2012).
- [19] Y. Zhang, W. S. Zhao, D. Ravelosona, J. O. Klein, J. V. Kim, and C. Chappert, Perpendicular-magnetic-anisotropy CoFeB racetrack memory, *J. Appl. Phys.* **111**, 093925 (2012).
- [20] Q. L. Lv, J. W. Cai, S. L. He, and L. Sun, Perpendicular magnetic anisotropy and magnetic proximity effect in $\text{Pt}_{1-\delta}\text{Fe}_\delta/\text{Co}$ multilayer films, *J. Magn. Magn. Mater.* **323**, 465 (2011).
- [21] G. Yu, Z. Wang, M. Abolfath-Beygi, C. He, X. Li, K. L. Wong, P. Nordeen, H. Wu, G. P. Carman, X. Han, I. A. Alhomoudi, P. K. Amiri, and K. L. Wang, Strain-induced modulation of perpendicular magnetic anisotropy in Ta/CoFeB/MgO structures investigated by ferromagnetic resonance, *Appl. Phys. Lett.* **106**, 072402 (2015).
- [22] A. W. Rushforth, E. De Ranieri, J. Zemen, J. Wunderlich, K. W. Edmonds, C. S. King, E. Ahmad, R. P. Campion, C. T. Foxon, B. L. Gallagher, K. Výborný, J. Kučera, and T. Jungwirt, Voltage control of magnetocrystalline

- anisotropy in ferromagnetic-semiconductor-piezoelectric hybrid structures, *Phys. Rev. B* **78**, 085314 (2008).
- [23] D. Lebeugle, A. Mougin, M. Viret, D. Colson, and L. Ranno, Electric Field Switching of the Magnetic Anisotropy of a Ferromagnetic Layer Exchange Coupled to the Multiferroic Compound BiFeO_3 , *Phys. Rev. Lett.* **103**, 257601 (2009).
- [24] B. Cui, C. Song, G. A. Gehring, F. Li, G. Wang, C. Chen, J. Peng, H. Mao, F. Zeng, and F. Pan, Electrical manipulation of orbital occupancy and magnetic anisotropy in manganites, *Adv. Funct. Mater.* **25**, 864 (2015).
- [25] J. Zhang, Z. Zhong, X. Guan, X. Shen, J. Zhang, F. Han, H. Zhang, H. Zhang, X. Yan, Q. Zhang, L. Gu, F. Hu, R. Yu, B. Shen, and J. Sun, Symmetry mismatch-driven perpendicular magnetic anisotropy for perovskite/brownmillerite heterostructures, *Nat. Commun.* **9**, 1923 (2018).
- [26] J. Wu, J. W. Lynn, C. J. Glinka, J. Burley, H. Zheng, J. F. Mitchell, and C. Leighton, Intergranular Giant Magnetoresistance in a Spontaneously Phase Separated Perovskite Oxide, *Phys. Rev. Lett.* **94**, 037201 (2005).
- [27] P. Wang, L. Yao, M. Wang, and W. Wu, XPS and voltammetric studies on $\text{La}_{1-x}\text{Sr}_x\text{CoO}_{3-\delta}$ perovskite oxide electrodes, *J. Alloys Compd.* **311**, 53 (2000).
- [28] M. Imamura, N. Matsabayashi, and H. Shimada, Catalytically active oxygen species in $\text{La}_{1-x}\text{Sr}_x\text{CoO}_{3-\delta}$ studied by XPS and XAFS spectroscopy, *J. Phys. Chem. B* **104**, 7348 (2000).
- [29] H. Jeen, W. S. Choi, J. W. Freeland, H. Ohta, C. U. Jung, and H. N. Lee, Topotactic phase transformation of the brownmillerite $\text{SrCoO}_{2.5}$ to the perovskite $\text{SrCoO}_{3-\delta}$, *Adv. Mater.* **25**, 3651 (2013).
- [30] M. Long, W. Cai, J. Cai, B. Zhou, X. Chai, and Y. Wu, Efficient photocatalytic degradation of phenol over $\text{Co}_3\text{O}_4/\text{BiVO}_4$ composite under visible light irradiation, *J. Phys. Chem. B* **110**, 20211 (2006).
- [31] N. Lu, et al., Electric-field control of tri-state phase transformation with a selective dual-ion switch, *Nature (London)* **546**, 124 (2017).
- [32] B. Cui, C. Song, F. Li, X. Y. Zhong, Z. C. Wang, P. Werner, Y. D. Gu, H. Q. Wu, M. S. Saleem, S. S. P. Parkin, and F. Pan, Electric-field Control of Oxygen Vacancies and Magnetic Phase Transition in a Cobaltite/Manganite Bilayer, *Phys. Rev. Appl.* **8**, 044007 (2017).
- [33] J. Song, Y. Chen, X. Chen, H. Wang, T. Khan, F. Han, J. Zhang, H. Huang, J. Zhang, H. Zhang, H. Zhang, X. Yan, S. Qi, F. Hu, B. Shen, R. Yu, and J. Sun, Tuning the Magnetic Anisotropy of $\text{La}_{2/3}\text{Sr}_{1/3}\text{MnO}_3$ by Controlling the Structure of SrCoO_x in the Corresponding Bilayers Using Ionic-Liquid Gating, *Phys. Rev. Appl.* **12**, 054016 (2019).
- [34] See Supplemental Material at <http://link.aps.org/supplemental/10.1103/PhysRevApplied.14.024062> for experimental details, XRR results, $M-T$ and $M-H$ curves for single LSMO and LSCO films, detailed $M-T$ curves for LSCO/LSMO bilayer films of different thicknesses and for the SL₁₀ sample in different gating states, and XAS spectra of the LSCO(4.5 nm)/LSMO(4.5 nm) bilayer in different gating states.
- [35] M. Martin, G. Shirane, Y. Endoh, K. Hirota, Y. Moritomo, and Y. Tokura, Magnetism and structural distortion in the $\text{La}_{0.7}\text{Sr}_{0.3}\text{MnO}_3$ metallic ferromagnet, *Phys. Rev. B* **53**, 14285 (1996).
- [36] R. Caciuffo, D. Rinaldi, G. Barucca, J. Mira, J. Rivas, M. A. Señarís-Rodríguez, P. G. Radaelli, D. Fiorani, and J. B. Goodenough, Structural details and magnetic order of $\text{La}_{1-x}\text{Sr}_x\text{CoO}_3$ ($x \leq 0.3$), *Phys. Rev. B* **59**, 1068 (1999).
- [37] M. Itoh, I. Natori, S. Kubota, and K. Motoya, Spin-glass behavior and magnetic phase diagram of $\text{La}_{1-x}\text{Sr}_x\text{CoO}_3$ ($0 \leq x \leq 0.5$) studied by magnetization measurements, *J. Phys. Soc. Jpn.* **63**, 1486 (1994).
- [38] B. Li, R. V. Chopdekar, A. M. Kane, K. Hoke, A. T. N'Diaye, E. Arenholz, and Y. Takamura, Thickness-dependent magnetic and electrical transport properties of epitaxial $\text{La}_{0.7}\text{Sr}_{0.3}\text{CoO}_3$ films, *AIP Adv.* **7**, 045002 (2017).
- [39] H. W. Yang, H. R. Zhang, Y. Li, S. F. Wang, X. Shen, Q. Q. Lan, S. Meng, R. C. Yu, B. G. Shen, and J. R. Sun, Anomalous magnetism in strained $\text{La}_{1-x}\text{Sr}_x\text{CoO}_3$ epitaxial films ($0 \leq x \leq 0.5$), *Sci. Rep.* **4**, 6206 (2014).
- [40] S. Carter, A. Selcuk, R. J. Carter, J. Kajda, J. A. Kilner, and B. C. H. Steele, Oxygen transport in selected nonstoichiometric perovskite-structure oxides, *Solid State Ionics* **53-56**, 597 (1992).
- [41] T. Matou, K. Takeshim, L. D. Anh, M. Seki, H. Tabata, M. Tanaka, and S. Ohya, Reduction of the magnetic dead layer and observation of tunneling magnetoresistance in $\text{La}_{0.67}\text{Sr}_{0.33}\text{MnO}_3$ -based heterostructures with a LaMnO_3 layer, *Appl. Phys. Lett.* **110**, 212406 (2017).
- [42] F. M. F. de Groot, J. C. Fuggle, B. T. Thole, and G. A. Sawatzky, $L_{2,3}$ x-ray-absorption edges of d^0 compounds: K^+ , Ca^{2+} , Sc^{3+} , and Ti^{4+} in O_h (octahedral) symmetry, *Phys. Rev. B* **41**, 928 (1990).
- [43] C. Aruta, G. Ghiringhelli, A. Tebano, N. G. Boggio, N. B. Brookes, P. G. Medaglia, and G. Balestrino, Strain induced x-ray absorption linear dichroism in $\text{La}_{0.7}\text{Sr}_{0.3}\text{MnO}_3$ thin films, *Phys. Rev. B* **73**, 235121 (2006).
- [44] P. Bruno, Tight-binding approach to the orbital magnetic moment and magnetocrystalline anisotropy of transition-metal monolayers, *Phys. Rev. B* **39**, 865 (1989).
- [45] P. Bruno, *Magnetismus Von Festkörpern und Grenzflächen, Ferienkurse des Forschungszentrums Jülich* (KFA, Jülich, Germany, 1993), Chap. 24, p. 1.
- [46] S. Valencia, Z. Konstantinovic, D. Schmitz, A. Gaupp, Ll. Balcells, and B. Martinez, Interfacial effects in manganite thin films with different capping layers of interest for spintronic applications, *Phys. Rev. B* **84**, 024413 (2011).
- [47] L. Wu, M. Chen, C. Li, J. Zhou, L. Shen, Y. Wang, Z. Zhong, M. Feng, Y. Zhang, K. Han, T. V. Venkatesan, S. J. Pennycook, P. Yu, J. Ma, X. R. Wang, and C.-W. Nan, Ferromagnetism and matrix-dependent charge transfer in strained LaMnO_3 - LaCoO_3 superlattices, *Mater. Res. Lett.* **6**, 501 (2018).
- [48] M. Merz, D. Fuchs, A. Assmann, S. Uebe, H. V. Löheneysen, P. Nagel, and S. Schuppler, Spin and orbital states in single-layered $\text{La}_{2-x}\text{Ca}_x\text{CoO}_4$ studied by doping- and temperature-dependent near-edge x-ray absorption fine structure, *Phys. Rev. B* **84**, 014436 (2011).
- [49] R. I. Dass and J. B. Goodenough, Multiple magnetic phases of $\text{La}_2\text{CoMnO}_{6-\delta}$ ($0 \leq \delta \leq 0.05$), *Phys. Rev. B* **67**, 014401 (2003).
- [50] J. B. Goodenough, *Magnetism and the Chemical Bond* (Wiley, New York, 1963), Chap. 3, p. B.